Arabian Journal of Geosciences (2021) 14: 520
https://doi.org/10.1007/s12517-021-06740-0

ORIGINAL PAPER

Bulk pyrolysis and biomarker fingerprints of Late Cretaceous Galhak Shale Formation in the northern Melut Basin, Sudan: implications on lacustrine oil-source rock

Mohammed Hail Hakimi[1] · Atif N. Abas[2] · Yousif T. Hadad[3] · Hussain J. Al Faifi[4] · Mostafa Kinawy[5] · Aref Lashin[5]

Received: 28 November 2020 / Accepted: 16 February 2021 / Published online: 15 March 2021

Abstract

Organic-rich shale samples from the Late Cretaceous Galhak Formation were collected from one well location in the northern Melut Basin, Sudan, and analyzed by integrated organic geochemical and microscopic techniques. The study investigates the nature and preservation conditions of the organic facies and their relevance to petroleum resource potential. Judging from the high total organic contents (total organic carbon (TOC) > 2%), the analyzed Galhak shales are organically rich and include favorable source rocks. The organic richness in these shale sediments may be attributed to enhance the preservation of organic matter under suboxic conditions as implied from the *n*-alkanes and isoprenoid biomarkers. Biological markers, including of *n*-alkanes, isoprenoids, terpanes, and steranes, further suggest that the Galhak shale sediments were deposited in a relatively fresh lacustrine environment and received largely aquatic organic matter of plankton and bacteria with little terrestrial plant input. An abundance of aquatic-derived organic matter is consistent with types I and II kerogen as indicated by high Rock-Eval HI values of more than 400 mg HC/g TOC. The hydrogen-rich kerogen types I and II in the analyzed samples suggests an oil-prone source. According to the optical and geochemical maturity indicators, the organic matter in the Galhak oil shale is thermally immature; thus, they have not reached sufficient oil-window maturity for commercial oil generation. Therefore, the deeper parts of the Melut Basin, where the Galhak Formation reached high mature of peak-oil generation window, are recommended for further petroleum exploration and production.

Keywords Galhak Formation · Oil-source rock · Types I and II kerogen · Northern Melut Basin · Sudan

Introduction

Sudan's interior contains several onshore sedimentary basins (Fig. 1), all of which are related to the rifting activities of the Western, Central, and East African Rift systems (Browne et al. 1985; Schull 1988). The Muglad and Melut onshore rift basins constitute the richest petroleum province in Sudan (Dou et al. 2007; Makeen et al. 2015a, b; 2016a, b). The Muglad Basin is an important hydrocarbon basin containing several hydrocarbon accumulations and several well-known oil fields (Makeen et al. 2015b). With its high potential for conventional petroleum exploration and development, the Muglad Basin has received attention of the petroleum industry and academic researchers (e.g., Dou et al. 2013; Makeen et al. 2015a, b, 2016a, b; Mohamed et al. 1999; Mohamed et al. 2000; Mohamed et al. 2002; Tong et al. 2004).

The Melut Basin, another important Sudanese rift basin, is the target of this study. This basin lies in the Upper Nile and

Responsible Editor: Santanu Banerjee

✉ Mohammed Hail Hakimi
ibnalhakimi@yahoo.com

[1] Geology Department, Faculty of Applied Science, Taiz University, 6803 Taiz, Yemen

[2] Rawat Petroleum Operation Company, Khartoum, Sudan

[3] Oil Exploration and Production Authority (OEPA), Ministry of Petroleum, HQ, Khartoum, Sudan

[4] Geology and Geophysics Department, College of Science, King Saud University, Riyadh, Saudi Arabia

[5] Petroleum and Natural Gas Engineering Department, College of Engineering, King Saud University, P.O. Box 800, Riyadh 11421, Saudi Arabia

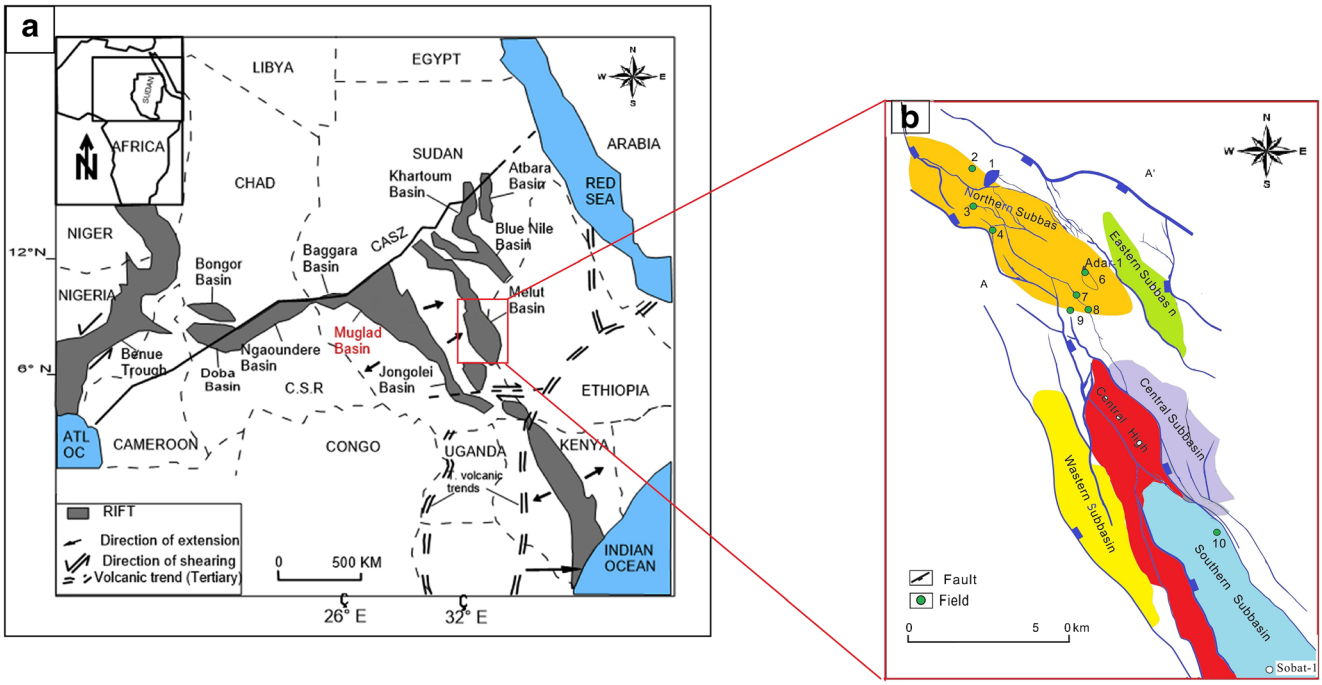

Fig. 1 (**A**) Regional tectonic map of western and central African rifted basins (modified from Makeen et al. 2016b), and (**B**) the Melut Basin, Sudan (modified from Dou et al. 2007)

Jonglei regions, south of the capital Khartoum, and east of the Nile River (Fig. 1A). It contains many oilfields (Fig. 1B), including the Great Palogue oilfield with estimated reserves of 900 million barrels (Dou et al. 2007). Although hydrocarbons exist in the Melut Basin, hydrocarbon exploration in this region began only recently, and data are scarce. Published research on the geochemical characteristics of source rocks in the Melut Basin and their relation to potential petroleum generation has been conducted and provided is limited (e.g., Dou et al. 2007). According to Dou et al. (2007), the main source rocks in the Melut Basin are the lacustrine shales of the Early Cretaceous Al-Gayger Formation; however, organic-rich shale intervals are found in the Late Cretaceous Galhak Formation and need to be studied. In parallel with previous studies of the organic-rich interval in the older Al-Gayger Formation (e.g., Dou et al. 2007), we considered characteristics of the organic-rich shale intervals within the Galhak Formation to obtain more information on the origin of organic matter in the Galhak shale intervals and gain deep insight into their hydrocarbon generation potential, with relevance to a broad perspective on exploring for conventional petroleum resources.

Using organic geochemical analyses coupled with the kerogen microscopic method, this study comprehensively investigates the source rock characteristics of the organic-rich shale intervals in the Late Cretaceous Galhak Formation. Samples were collected from a well in the northern Melut Basin. The aim is to understand the richness of organic matter, the nature of the organic facies, and their connection to the oil-source rock potential. In addition, the nature and environmental conditions of deposition associated with the organic matter sources, the biomarker results of the aliphatic fraction are integrated into the bulk geochemical and visual kerogen data.

Geological setting

The Melut rift basin extends over 33,000 km^2. With a maximum width of 100 km and a length exceeding 310 km (Dou et al. 2007), it ranges from southeast Sudan to central Ethiopia (Fig. 1A). The Melut Basin is defined as an intracontinental Cretaceous–Tertiary rift basin resulting from strike-slip movement (Binks and Fairhead 1992; Genik 1993; Guiraud and Maurin 1992). Rifting began in the Early Cretaceous (Guiraud and Maurin 1992; McHargue et al. 1992) creating several sub-basin rift systems in the Melut Basin, namely, the Northern, Eastern, Central, Western, and Southeastern (Fig. 2A) sub-basins characterized by downwarped, horst, and tilted blocks (Fig. 2B), which developed favorable structural traps for hydrocarbons. These structural traps formed during the Early Cretaceous and evolved during the Tertiary (Genik 1993; Guiraud and Maurin 1992; McHargue et al. 1992).

The Melut Basin contains up to 10 km of sediments (Dou et al. 2007), ranging in age from Early Cretaceous to Quaternary (Fig. 3). The older exposed sedimentary rock is represented by the Early Cretaceous Al-Gayger Formation (Fig. 3) resting on Precambrian basement rocks with an unconformable content. The Al-Gayger Formation is divided

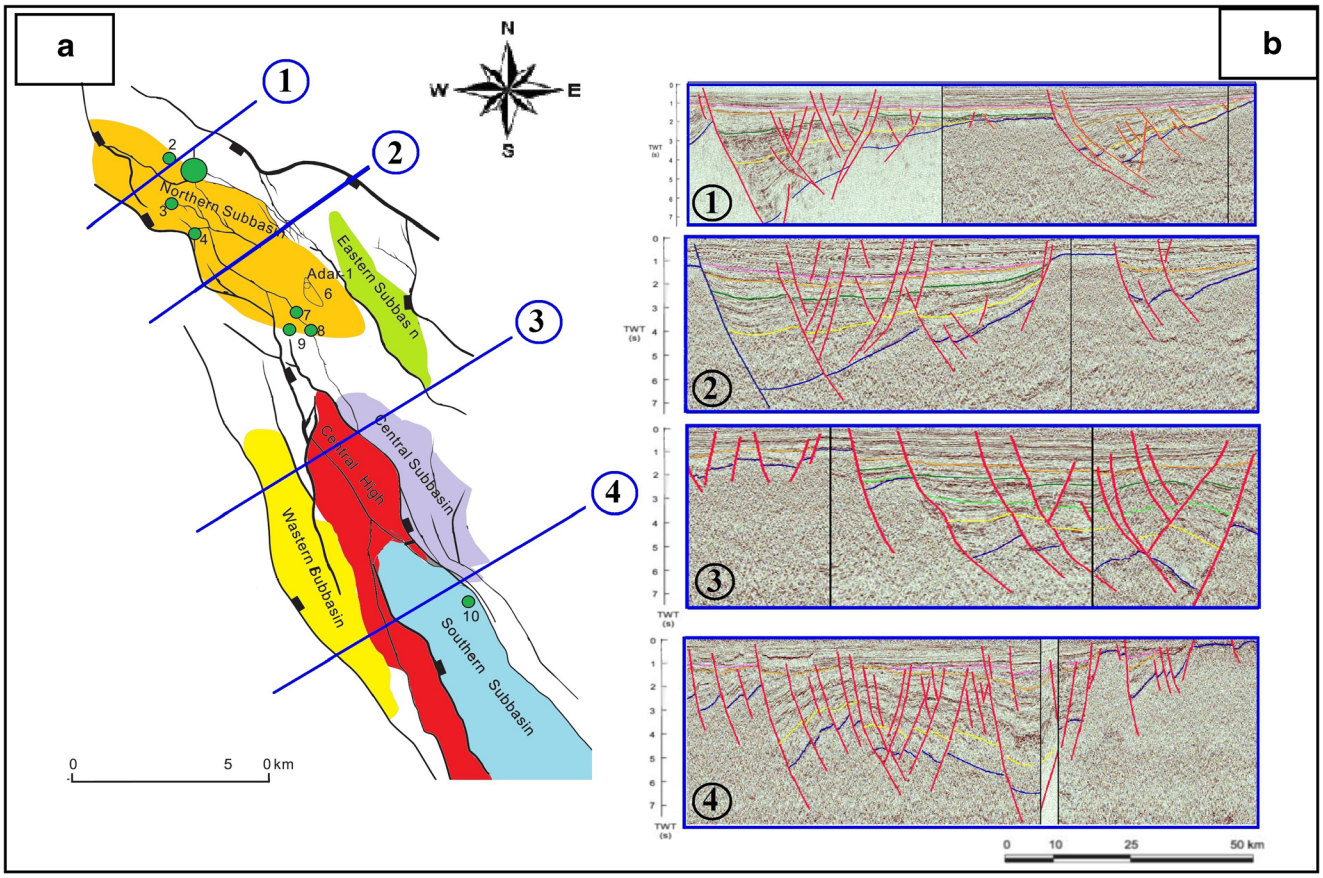

Fig. 2 (**A**) Map view of major faults in the Melut Basin (modified from Dou et al. 2007), and (**B**) several cross-sections showing the structural setting of hydrocarbons across the Melut Basin

into two units varying from fluvial–deltaic to lacustrine in their sedimentary environment (Dou et al. 2007). The lower unit is mainly composed of thin sandstones that are interbedded with thin claystones, whereas the upper unit contains dark gray and black dense shales with interbedded thin sandstones (Fig. 3). The upper part, representing the semi-deep and deep lacustrine sediments, containing proven source rocks in the Melut Basin (Dou et al. 2007). The Al-Gayger Formation is accompanied by thick sediments from the Late Cretaceous Galhak and Melut Formations (Fig. 3). These sediments are mainly sandstones with interbedded shales of the Galhak and Melut Formations, indicating a depositional environment ranging from deltaic/fluvial to shallow lacustrine (Dou et al. 2007). The Galhak Formation lies on the Al-Gayger shales with an unconformable contact of late Senomanian to Turonian age (Dou et al. 2007), which was formed in braided delta to shallow lake environments (Dou et al. 2007).

The Late Cretaceous Melut Formation was followed by mixed sandstone and claystone clastic sediments of the Tertiary megasequence with an unconformable contact (Fig. 3). The Tertiary megasequence comprises the Samma, Yabus, Adar, Jimidi, Lau, Miadol, and Daga Formations (Fig. 3). The Tertiary sediments are mainly composed of sandstones and siltstones with interbedded claystones and shales. They were deposited during the Paleocene–Pliocene (Fig. 3), although the Cretaceous Melut and Paleocene Samma and Yabus sandstones in the Melut Basin are primarily considered petroleum reservoirs (Fig. 3). The overlying Eocene Adar Formation mainly comprises sediments such as shales and claystones, providing excellent regional seal rocks for the underlying Cretaceous and Paleocene oil-bearing reservoir rocks (Fig. 3). The Quaternary-dated Agor Formation is the youngest stratigraphic formation in the basin that mainly comprises sandstones (Fig. 3) and that unconformably covers the Late Miocene–Pliocene Daga Formation.

Samples and methods

The Melut Basin is still under hydrocarbon exploration and the available samples for the Galhak Formation the basin are limited, where the drilled wells are also limited. In this regard, thirteen cuttings samples were collected from the shale intervals of the Late Cretaceous Galhak Formation in a well located in the northern Melut Basin (Table 1). Prior to analysis, the cuttings were washed with cold water to remove contaminants from drilling mud and other drilling additives present.

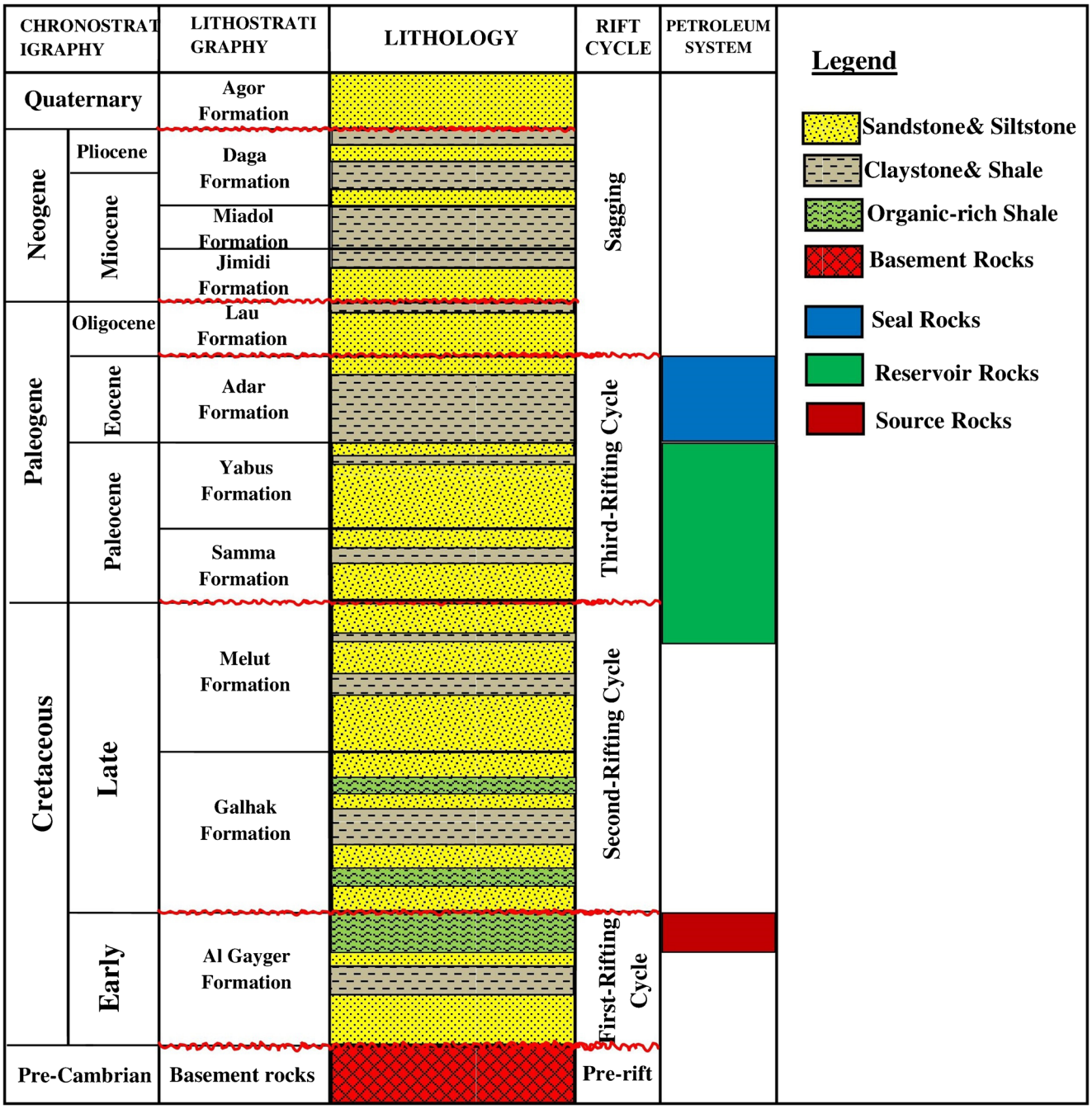

Fig. 3 Generalized stratigraphic column of the Cretaceous–Quaternary sequences of the Melut Basin, including the petroleum system elements

The cuttings samples were finely milled (60 μm) for TOC content determination using a LECO CS-125 instrument. Of these samples, seven samples were subsequent screened using a Rock-Eval II instrument to determine the basic source rock parameters. These parameters include S_1 (amount of free hydrocarbons), S_2 (amount of hydrocarbons generated by thermal cracking of non-volatile organics), S_3 (amount of CO_2 generated by kerogen pyrolysis), and T_{max} (temperature of maximum hydrocarbon release by kerogen cracking) of the samples were measured during pyrolysis. The geochemical parameters—hydrogen index (HI), oxygen index (OI), potential yield (PY), and production index (PI)—were calculated (see Table 1) as defined by Espitalie et al. (1977, 1985), and Peters and Cassa (1994).

Four representative shale samples were selected for further various organic geochemical analyses: extraction and fractionation of bitumen, and gas chromatography and gas chromatography–mass spectrometry (GC–MS) of the saturated hydrocarbon fraction. In addition, their vitrinite reflectance was measured and their kerogen was visually examined. The

Table 1 Rock-Eval pyrolysis and TOC data and Kerogen typing (i.e., vitrinite, inertinite, and sapropel %) and vitrinite reflectance (%VRo) results for representative Late Cretaceous shale samples in the Well A, northern Melut Basin, Sudan

Wells	Depth (MD)	TOC wt.%	Rock-Eval pyrolysis									Kerogen typing (%) (transmitted light)			VRo (%) (reflected light)
			S_1 (mg/g)	S_2 (mg/g)	S_3 (mg/g)	T_{max} (°C)	HI (mg/g)	OI (mg/g)	PY (mg/g)	PI (mg/g)	S_2/S_3 (mg/g)	Vitrinite	Inertinite	Sapropel	
Well A	1990	2.58	0.45	14.29	1.78	442	554	69	14.74	0.03	8.03				
	2010	4.88													
	2020	5.02	0.82	26.56	1.91	445	529	38	27.38	0.03	13.91	Trace	Trace	100	
	2030	4.82													
	2040	4.52													
	2050	4.29	1.10	26.25	1.37	444	612	32	27.35	0.04	19.16	Trace	Trace	100	
	2060	5.08	0.92	29.82	1.17	447	587	23	30.74	0.03	25.49				
	2070	2.91										5	Trace	95	0.47
	2080	2.24	0.46	10.44	1.16	442	466	52	10.9	0.04	9.00				
	2090	2.49										10	5	85	0.46
	2100	2.52	0.40	11.39	1.41	441	452	56	11.79	0.03	8.08				
	2110	4.69	0.85	25.09	2.11	438	535	45	25.94	0.03	11.89				

TOC, total organic carbon, wt.%; S_1, volatile hydrocarbon (HC) content, mg HC/g rock; S_2, remaining HC generative potential, mg HC/g rock; S_3, carbon dioxide content, mg CO_2/g rock; T_{max}, temperature at maximum of S_2 peak; *OI*, oxygen index = $S_3 \times 100$/TOC, mg CO_2/g TOC; *HI*, hydrogen index = $S_2 \times 100$/TOC, mg HC/g TOC; *PY*, potential yield = S_1+S_2 (mg/g); *PI*, production index = $S_1/(S_1+S_2)$

samples were selected based on their Rock-Eval pyrolysis results.

After grinding, the bitumen in the analyzed four shale samples was extracted using a solvent of DCM and methanol (CH_3OH) for 72 h. The extracted bitumen was then separated into aliphatic, aromatic, and polar fractions using liquid column chromatography with silica gel topped with alumina oxide. The aliphatic fraction of the samples was analyzed using a flame ionization detector gas chromatograph. The furnace temperature of the gas chromatograph was programmed between 140°C and 211 °C at a rate of 1 °C/min and held at 300 °C for 10 min.

Additionally, the saturated fraction of three extracted samples was analyzed with a gas chromatography–mass spectrometry (GC–MS) equipped. The flame ionization detector of GC-MS experimental analysis was operated in an HP–DB5–MS column with a distance of 30 m, an interior diameter of 0.30 mm, and a film thickness of 0.25 μm. The furnace temperature was programmed between 50°C and 180 °C at a rate of 3 °C/min and held at 300 °C for 25 min.

The terpane and sterane biomarkers were estimated by integrating the *m/z* 191 and *m/z* 217 ions, respectively, using Chemstation software. The biomarker compounds were selected based on retention times and mass spectra reported in published works such as Hakimi et al. (2020), Makeen et al. (2015a), and Philp (1985). Biomarker ratios were calculated using peak heights.

The organic geochemical analyses of the four representative shale samples were augmented through microscopic observations, including visual kerogen microscopy and reflectance measurements of the vitrinite organic matter using a Leitz Dialux/Laborlux microscope and a Leitz Orthoplan/MPV photometry system.

Microscopic examination of visual kerogen was prepared using standard palynological procedures; however, oxidation or acetolysis were omitted. Acid maceration requires hot hydrochloric acid (30% HCl) to dissolve the carbonates and hot hydrofluoric acid (60% HF) to extract or break down the silicates. Mineral residues were isolated from the kerogen using combined ultrasonic vibration and flotation in zinc bromide. The kerogen residues were categorized by placing them in glycerin jelly on glass slides and examining them under transmitted light using a Leitz Dialux/Laborlux microscope.

The vitrinite reflectance (%VRo) of two samples was analyzed using the polished block technique. The whole cutting samples were rough-crushed to approximately pea-sized fragments (2–3 mm) and then coated with epoxy resin. The VRo was measured using standard methods as described by Taylor et al. (1998). The analysis was conducted using oil immersion with a Zeiss microscope fitted with a Leitz Orthoplan/MPV photometry device under reflected light. The reflectance was calibrated on glasses and gemstones in the VRo range of 0.2–5.1%.

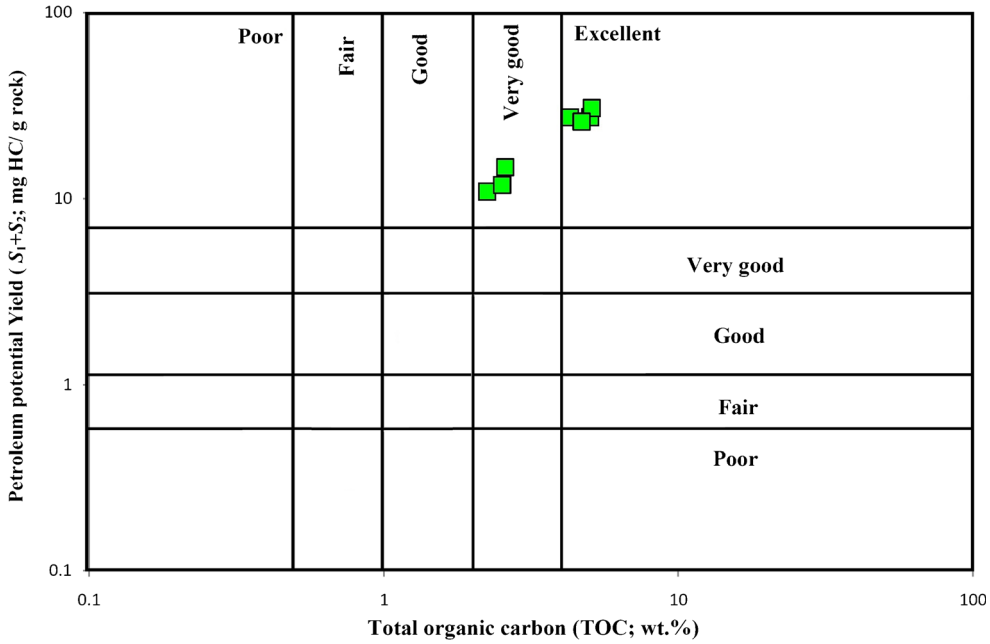

Fig. 4 Geochemical correlation between total organic matter (TOC) content and potential petroleum yield (S_1+S_2). The analyzed shale samples are very good to excellent potential source rocks for petroleum generation

Results and discussion

Richness of organic matter and generative potential

The richness of organic matter content, and contributing to petroleum generation potential during maturation was primarily evaluated using TOC content (Peter and Cassa 1994). From the weight percentage of the TOC content, we can assess the organic richness in a source rock (Bissada 1982; Peter and Cassa 1994; Katz and Lin 2014).

In this study, TOC and Rock-Eval pyrolysis results are shown in Table 1 and used to evaluate the amount of organic matter in the analyzed shale samples from the Galhak Formation and their generative potential. In this regard, the

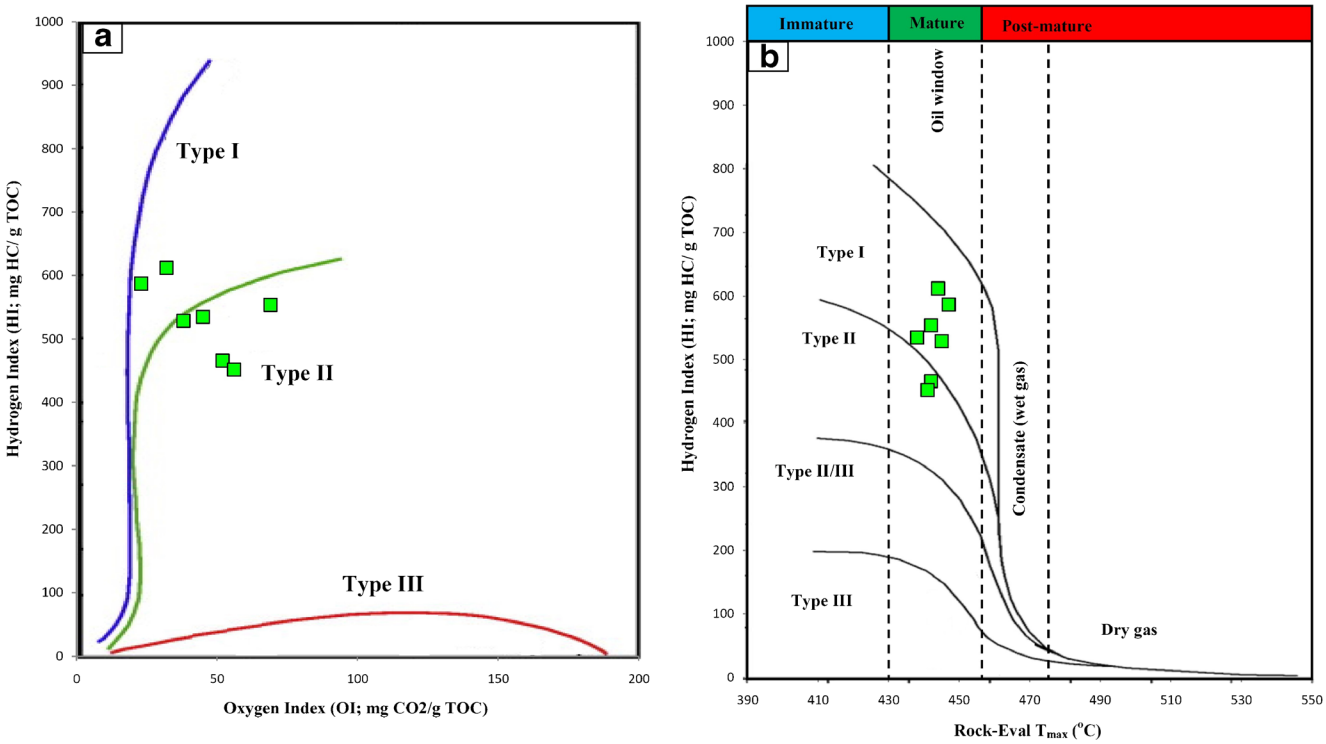

Fig. 5 Geochemical correlations between hydrogen index (HI), oxygen index (OI), and T_{max}. The analyzed shale samples are dominated by type I and type II KEROGENS

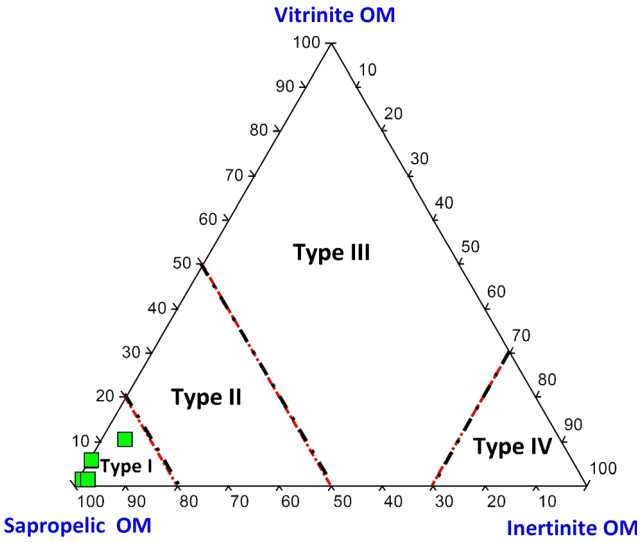

Fig. 6 Ternary plot of the dominant kerogen assemblages recognized in the samples from the well in Galhak shale, showing the dominance of type I kerogen

TOC contents of the analyzed Galhak shales ranged from 2.24 to 5.08%. Therefore, the analyzed Galhak shales are considered to have probably high potential as source rocks, with the TOCs exceeding 2% (Bissada 1982). TOC content alone is not enough to satisfy all the requirements of a generative potential and must be collaborated with the Rock-Eval S_2 yield (e.g., Peters 1986; Peters and Cassa 1994; Dembicki 2009). The analyzed shale samples exhibited high total hydrocarbon yields from kerogen cracking (S_2) in the range of 10.44–29.82 mg HC/g rock (Table 1). The high S_2 yields concur with the TOC results and show that most of the analyzed shale samples of the Galhak Formation attained very good to excellent source rock potential for hydrocarbon generation (Fig. 4).

Kerogen characteristics

Quantitative and qualitative results of organic type were geochemically and optically investigated throughout this study

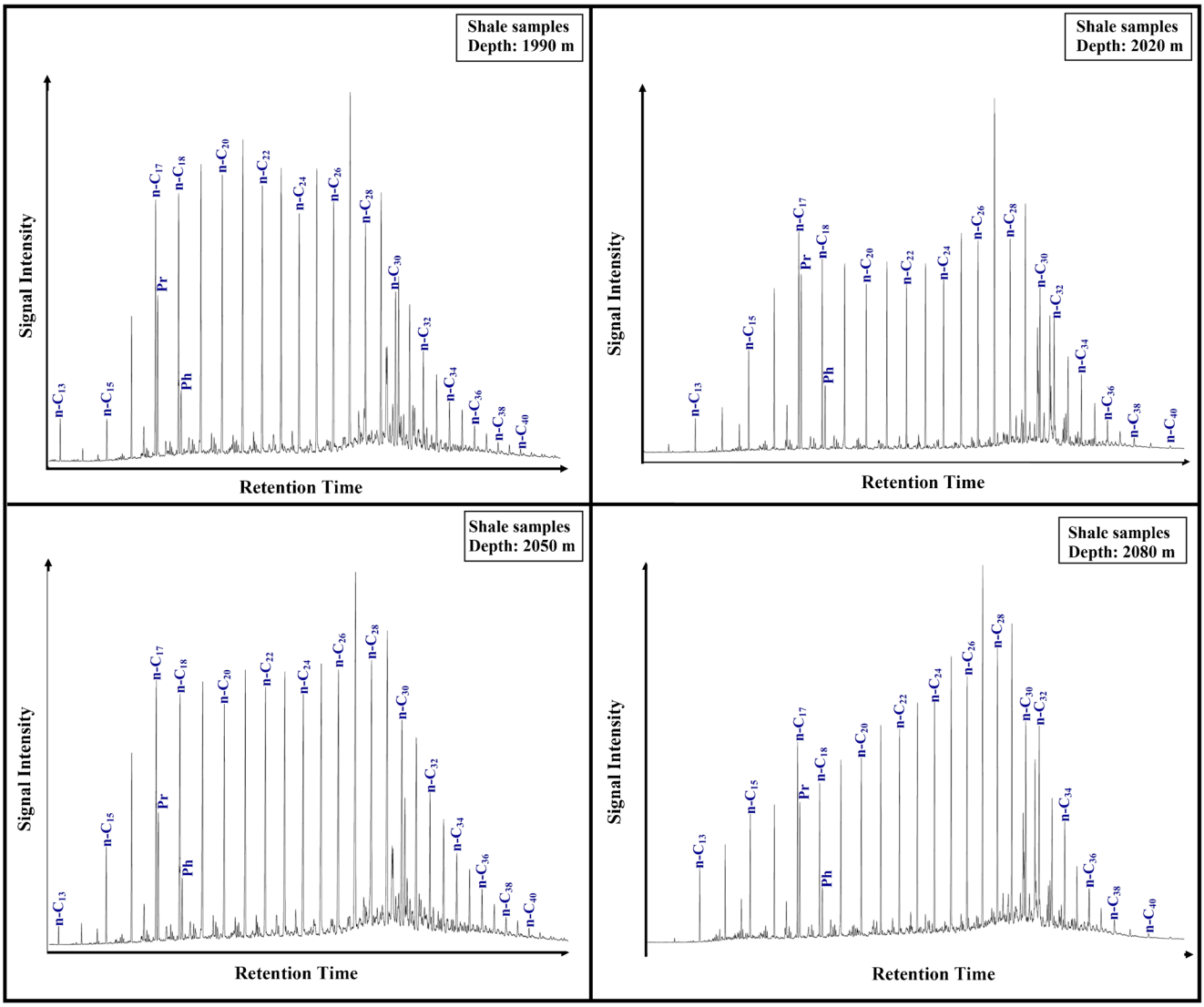

Fig. 7 Gas chromatograms of the saturated hydrocarbon fractions in four analyzed shale samples

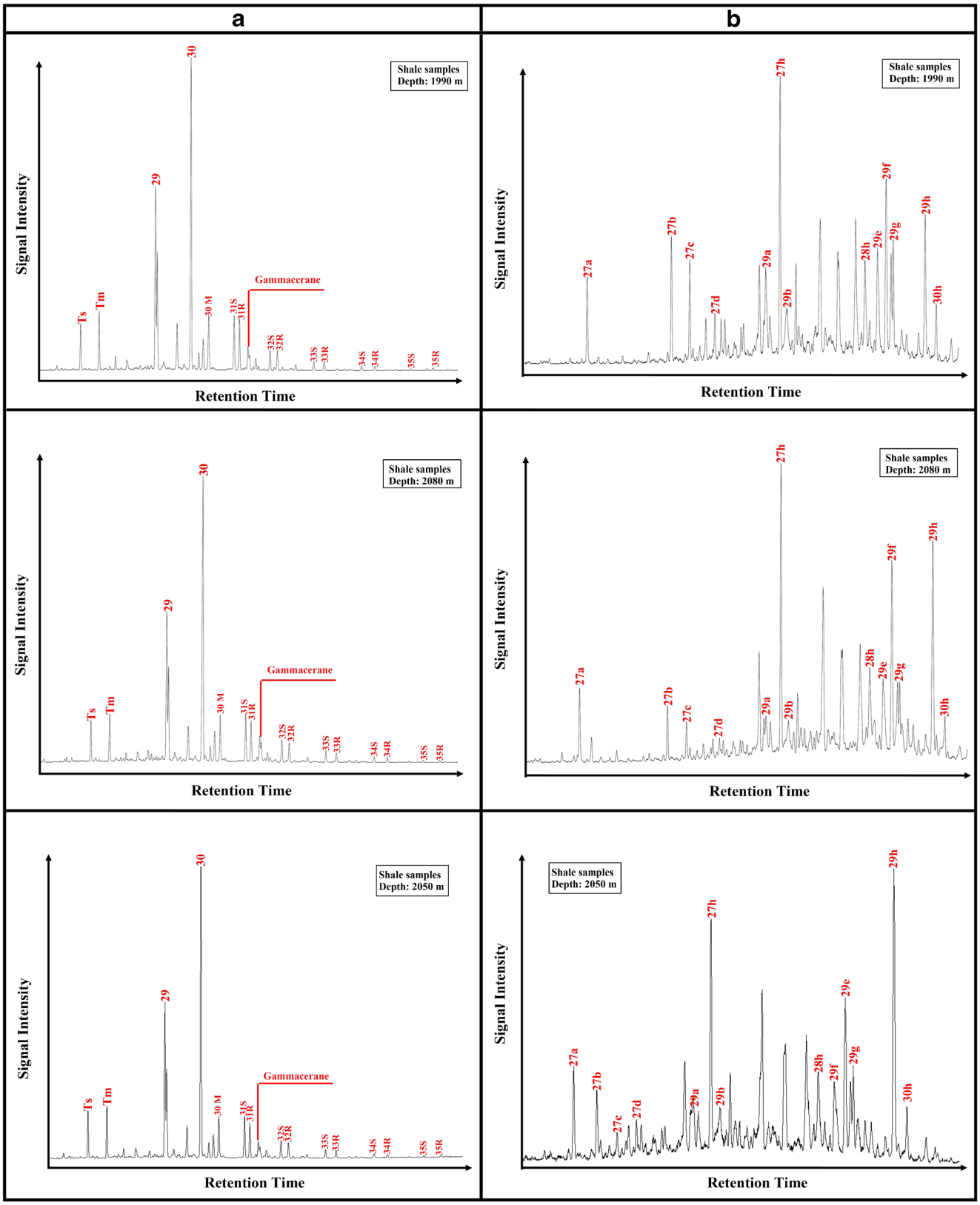

Fig. 8 Distributions of terpanes, steranes, and diasteranes in the *m/z* 191 and *m/z* 217 mass fragmentograms, obtained from the saturated fractions of three analyzed shale samples

Table 2 Selected biomarker parameters of the representative Late Cretaceous shale samples in the Well A, northern Melut Basin, Sudan, illustrating source organic matter, depositional environment conditions, and thermal maturity

No.	Depth (m.)	*n*-Alkane and isoprenoids				Triterpanes and terpanes (*m/z* 191)						Steranes (m/z217)					
		Pr/Ph	Pr/C_{17}	Ph/C_{18}	CPI	C_{32} 22S/(22S + 22R)	C_{29}/C_{30}	Ts/Tm	G/C_{30}	M_{30}/C_{30}	HCR_{31}/HC_{30}	C_{29} 20S/20S+20R	C_{29} ββ/(ββ+αα)	C_{27}/C_{29} regular steranes	Regular steranes (%)		
															C_{27}	C_{28}	C_{29}
Well A	1990	2.37	0.77	0.31	1.35	0.49	0.58	0.78	0.09	0.19	0.16	0.40	0.42	1.21	47.10	14.10	38.80
	2020	2.55	1.08	0.50	1.31												
	2050	1.97	0.52	0.28	1.34	0.50	0.54	0.88	0.06	0.19	0.11	0.30	0.40	0.87	40.49	12.96	46.55
	2080	2.57	0.93	0.46	1.23	0.50	0.52	0.81	0.09	0.16	0.14	0.36	0.41	1.24	40.80	26.40	32.80

Pr, pristane; *Ph*, phytane; *Tm*, (C_{27} 17α(H)-22,29,30-trisnorhopane); *Ts*, (C_{27} 18α(H)-22,29,30-trisnorneohopane); *CPI*, carbon preference index (1): {2(C_{23} + C_{25} + C_{27} + C_{29}) / (C_{22} + 2[C_{24} + C_{26} + C_{28}] + C_{30})}; HCR_{31}/HC_{30}, C_{31} regular homohopane/C_{30} hopane, C_{29}/C_{30}: C_{29} norhopane/C_{30} hopane; G/HC_{30}, gammacerane/C_{30} hopane, M_{30}/C_{30}= C_{30} moretane/C_{30} hopane

(Table 1). From these results, we can assess the kerogen types and their characteristics, representing the source of organic matter input in the analyzed shale samples.

The qualitative organic type (bulk kerogen) in the analyzed shale samples was evaluated based on their geochemical parameters of Rock-Eval HI and OI (Espitalie et al. 1985; Peters and Cassa 1994; Mukhopadhyay et al. 1995).

The analyzed shale sediments are dominated by HI with values between 452 and 612 mg HC/g TOC, and underwent minimal kerogen oxidation, as evidenced by their relatively low OI values (<69 mg CO_2/g TOC; see Table 1). Therefore, both HI and OI parameters were useful for classifying the bulk kerogen in the analyzed Galhak shales. Based on the overall Rock-Eval results, the analyzed samples mainly fell into types I and II kerogen, as obtained from the modified van Krevelen diagram of HI against OI (Fig. 5A). A modified-HI versus T_{max} plot further confirmed that the analyzed shale samples are dominated by kerogen of types I and II (Fig. 5B).

The derived organic facies are compatible with the optical application for obtaining the quantitative organic matter type under microscope, and provides accurate and more reliable assessments of the kerogen type (e.g., Makeen et al. 2015a, b; Abdullah et al. 2017). Table 1 shows summary the kerogen microscopic results, including the organic facies in the analyzed samples. The kerogen assemblages in the analyzed shales were dominated by primarily sapropelic organic matter, with volumes up to 85%. Several analyzed samples also contain minor amounts of vitrinite and inertinite organic matter in the range of 5–10% (Table 1). The high organic sapropelic matter is compatible with the presence of oil-prone kerogen. This inference of the kerogen characteristics is further supported by the distribution of kerogen assemblages (Cornford 1979). The distributions of sapropelic, vitrinite, and inertinite organic matter in the analyzed shale samples (Table 1) are plotted on the ternary diagram of Cornford (1979), and indicate that the organic facies in the analyzed shales predominantly belong to type I kerogen (Fig. 6).

Biomarker fingerprints and their relevance to organic matter inputs and preservation conditions

The nature of the organic matter and preservation conditions of the Galhak shales Formation were assessed using biomarkers and their proportions and parameters (e.g., Huang and Meinschein 1979; Volkman 1986; Waples and Machihara 1991).

The saturated hydrocarbon gas chromatograms and the GC–MS mass fragmentograms of the *m/z* 191 and *m/z* 217 ions are presented in Figs. 7 and 8.

The chromatograms of most of the analyzed shale samples show a unimodal distribution of normal alkanes between C_{13} and C_{36}, with elevated of mid length chain (C_{18}–C_{27}) *n*-alkanes (Fig. 7), suggesting a mixture of organic matter in the analyzed samples with high abundance of aquatic organic matter and

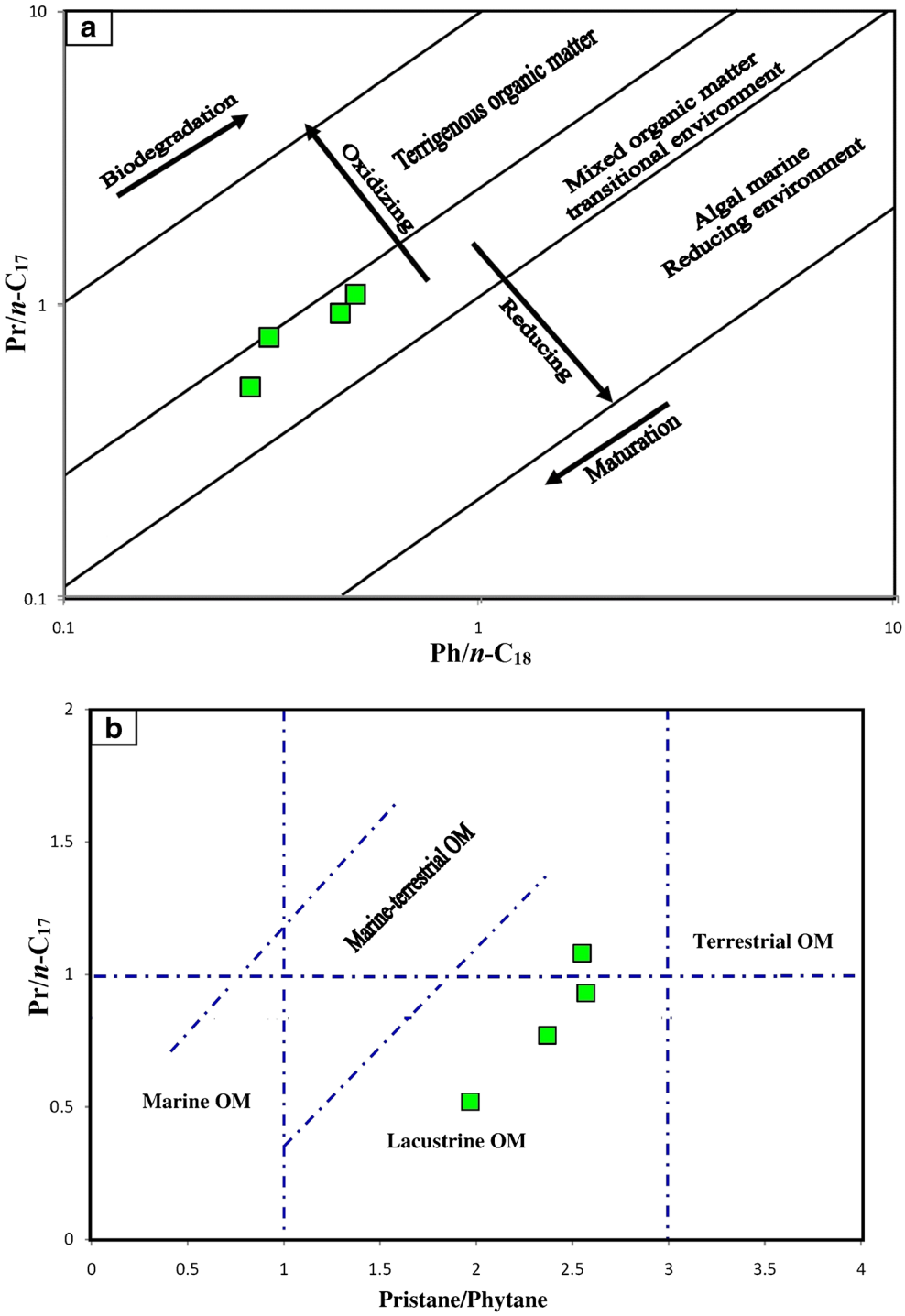

Fig. 9 Biomarker cross-plots of isoprenoid ratios: Pr/Ph, Pr/C_{17}, and Ph/C_{18}, showing mixed organic matter deposited in a lacustrine environment under suboxic conditions

significant amounts of land plants. However, this distribution of normal alkanes further displays a relatively high carbon preference index in the range of 1.23–1.35 (Table 2).

In addition, the chromatograms of the analyzed shale samples contained significant amounts of the acyclic isoprenoid hydrocarbons, i.e., pristane (Pr) and phytane (Ph) (Fig. 7). The chromatograms also revealed a predominance of Pr over Ph (Fig. 7), resulting in relatively high Pr/Ph ratios between 1.97 and 2.57 (Table 2). The isoprenoid ratios relative to the *n*-alkane concentrations (Pr/*n*-C_{17} and Ph/*n*-C_{18}) were found to be in the range of 0.52–1.08 and 0.28–0.50, respectively (Table 2). The isoprenoids and their ratios are the most commonly used as indicators for the redox conditions and inputs of organic matter in depositional environments (e.g., Chandra et al. 1994; Didyk et al. 1978). In this regard, the relatively high ratios of Pr/Ph, pristane/*n*-C_{17}, and phytane/*n*-C_{18} suggest that a

mixture of organic matter deposited in lacustrine environment under suboxic to relatively oxic conditions (Fig. 9).

The GC–MS mass fragmentograms of the *m/z* 191 and *m/z* 217 ions affirmed the presence of hopanoids and steroids (Fig. 8) and were further used to provide specific information on the nature of organic matter and sedimentary environmental conditions (Huang and Meinschein 1979; Burwood et al. 1992; Hanson et al. 2000; Marynowski et al. 2000). The mass fragmentogram of *m/z* 191 reveals a higher proportion of hopanes than tricyclic terpanes (Fig. 8A). The identified hopanoid components included C_{30} hopane, C_{29} norhopane, 17α (H)-trisnorneohopane (Tm), 18α (H)-trisnorneohopane (Ts), and C_{31}–C_{35} homohopanes. The C_{30}-hopanes dominated over the C_{29} norhopanes (Fig. 8A), with C_{29}/C_{30} ratios less than 1 (Table 2). Such low C_{29}/C_{30} ratios imply that the lithofacies are clay-rich sediments (e.g., Gürgey 1999). In particular, C_{31} dominated the homohopane distributions; however, its proportion gradually decreased with the increasing carbon content (Fig. 8A). Meanwhile, the C_{31} 22R-series homohopanes were less abundant than C_{30} hopane (Fig. 8A) as evidenced by the low C_{31} 22R homohopane/C_{30} hopane ($C_{31}R/C_{30}H$) ratios between 0.11 and 0.16 (see Table 2). The low C_{31}-22R homohopane/C_{30}-hopane (C_{31R}/C_{30H}) ratios are consistent with the accumulation of mixed organic matter in a lacustrine depositional environment as demonstrated from the combination of the Pr/Ph and C_{31R}/C_{30H} ratios (Fig. 10).

Moreover, the low amounts of gammacerane were also recorded in the *m/z* 191 mass fragmentogram of the analyzed samples (Fig. 8A), yielding low gammacerane/C_{30} hopane ratios between 0.06 and 0.09 (Table 2). The presence of gammacerane derivatives is characteristic of either hypersalinity or water column stratification during deposition (Moldowan et al. 1985; ten Haven et al. 1989; Sinninghe Damsté et al. 1995). In the analyzed samples, the low amounts of gammacerane in *m/z* 191 fragmentograms (Fig. 9) and the gammacerane/C_{30}-hopane suggest that the analyzed shale samples were in relatively fresh lacustrine environment.

Sterane and diasterane biomarker compounds were found in the *m/z* 217 mass fragmentograms of the analyzed shale samples (Fig. 8B). Sterane was abundant in the aliphatic hydrocarbons of the samples (Fig. 8B). Among the regular C_{27}–C_{29} steranes, the C_{27} and C_{29} steranes were more abundant than regular C_{28} steranes (see the steroid distributions in Fig. 8B). The relative abundances of C_{27}, C_{28}, and C29 regular steranes were 38.52–47.10%, 11.90–26.40%, and 32.90–49.58%, respectively (Table 2).

The distribution of these regular steranes (C_{27}–C_{29}) when plotted on a Huang–Meinschein ternary diagram (1979) provide evidence for the high contributions of planktonic and bacterial organic matter in the analyzed samples (Fig. 11). The plot of C_{27}/C_{29} regular sterane and Pr/Ph ratios further indicted evidence of high contributions of aquatic organic matter (Fig. 12).

These recognized organic facies are also consistent with the results of the geochemical and visual kerogen analyses (Table 1). The Rock-Eval results reveal rich organic matter in the Galhak Formation samples that are dominated by types I and II kerogen (Fig. 5). An abundance of these kerogen types indicates a dominance of algal and bacteria organic matters (Taylor et al. 1998; Hakimi et al. 2012, 2016). The large quantities of organic matter derived from phytoplankton algae and microorganisms are further indicated by the

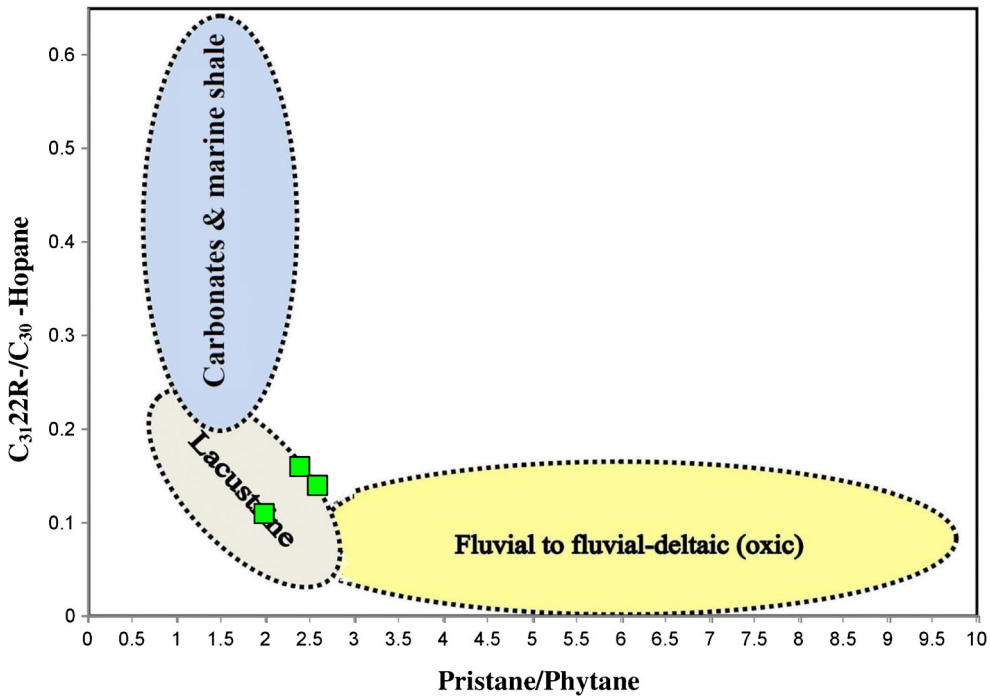

Fig. 10 Cross-plot of pristane/phytane ratio versus C_{31} R/C_{30} hopane ratio, confirming that the analyzed shale samples were deposited in a lacustrine environment

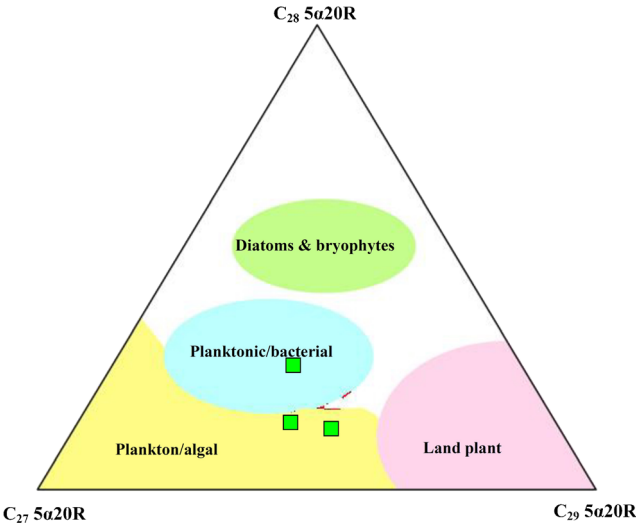

Fig. 11 Ternary diagram of regular steranes (C_{27}–C_{29}) relating the sterane compositions to the organic matter input (modified after Huang and Meinschein 1979)

predominance of sapropelic organic matter observed under the microscope (Table 1; Fig. 6).

Thermal maturation of organic matter

The level of thermal maturity of the organic matter in the Galhak shale analyzed in this study was assessed based on the several maturity indicators, including Rock-Eval geochemical T_{max} and production index (PI), vitrinite reflectance (%VRo) (Table 1), and biomarker parameters (Table 2).

The most accurate maturity indicator was vitrinite reflectance (%VRo), which provides valuable information on organic maturation and the evolution of petroleum generation (Teichmüller et al. 1998; Sweeney and Burnham 1990; Waples 1994). The VR values ranged from 0.43 to 0.47% (Table 1), confirming that the analyzed samples are immature.

Temperature of the maximum pyrolysis rate (T_{max}) is a commonly used measure of maturity (Bordenave et al. 1993; Peters 1986; Tissot et al. 1987). As kerogen matures, its T_{max} increases. During pyrolysis analysis, the T_{max} of the analyzed samples was determined as 438°C–447°C (Table 1), suggesting early to peak maturity of the oil window (Fig. 6B).

Along with the VRo values, the PI values of the analyzed samples were deemed sufficiently accurate for maturity evaluation. The PI values were 0.03–0.04 (Table 1), confirming the presence of immature organic matter (Peters and Cassa 1994; Fatma and Sadettin 2013). Furthermore, the lower S_1 values compared with S_2 (Table 1) indicate that the analyzed samples have not yet generated oil because of the low thermal maturation level.

The thermal maturity level of organic matter in the analyzed samples was determined from the biomarkers in the aliphatic hydrocarbon fraction, namely, the 22S/(22S + 22R) ratio of C_{32} homohopanes, the moretane to hopane (C_{30}M/C_{30}H) ratio, Ts/Tm, and the 20S/(20S+20R), and ββ/(ββ+αα) ratios of C_{29} sterane (Table 2).

The biomarker ratios of C_{32} hopane 22S/(22S+22R) and C_{29} sterane 20S/(20S+20R), and ββ/(ββ+αα) as well as Ts/Tm indicate maturity levels over the early mature range with increasing maturity (e.g. Seifert and Moldowan 1978, 1981, 1986; Roushdy et al. 2010; El Nady et al. 2014), whereas the low CM_{30}/C_{30} values further indicate mature source rocks (Mackenzie et al. 1980).

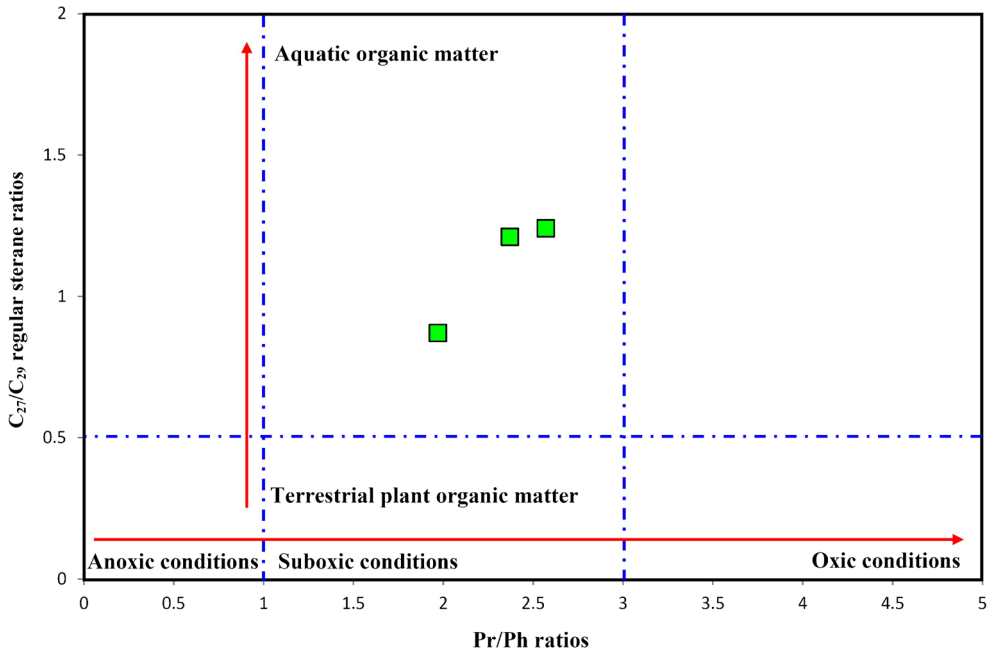

Fig. 12 Cross-plot of pristane/phytane ratio versus C_{22}/C_{29} regular steranes ratio, providing further evidence of high amounts of aquatic organic matter input

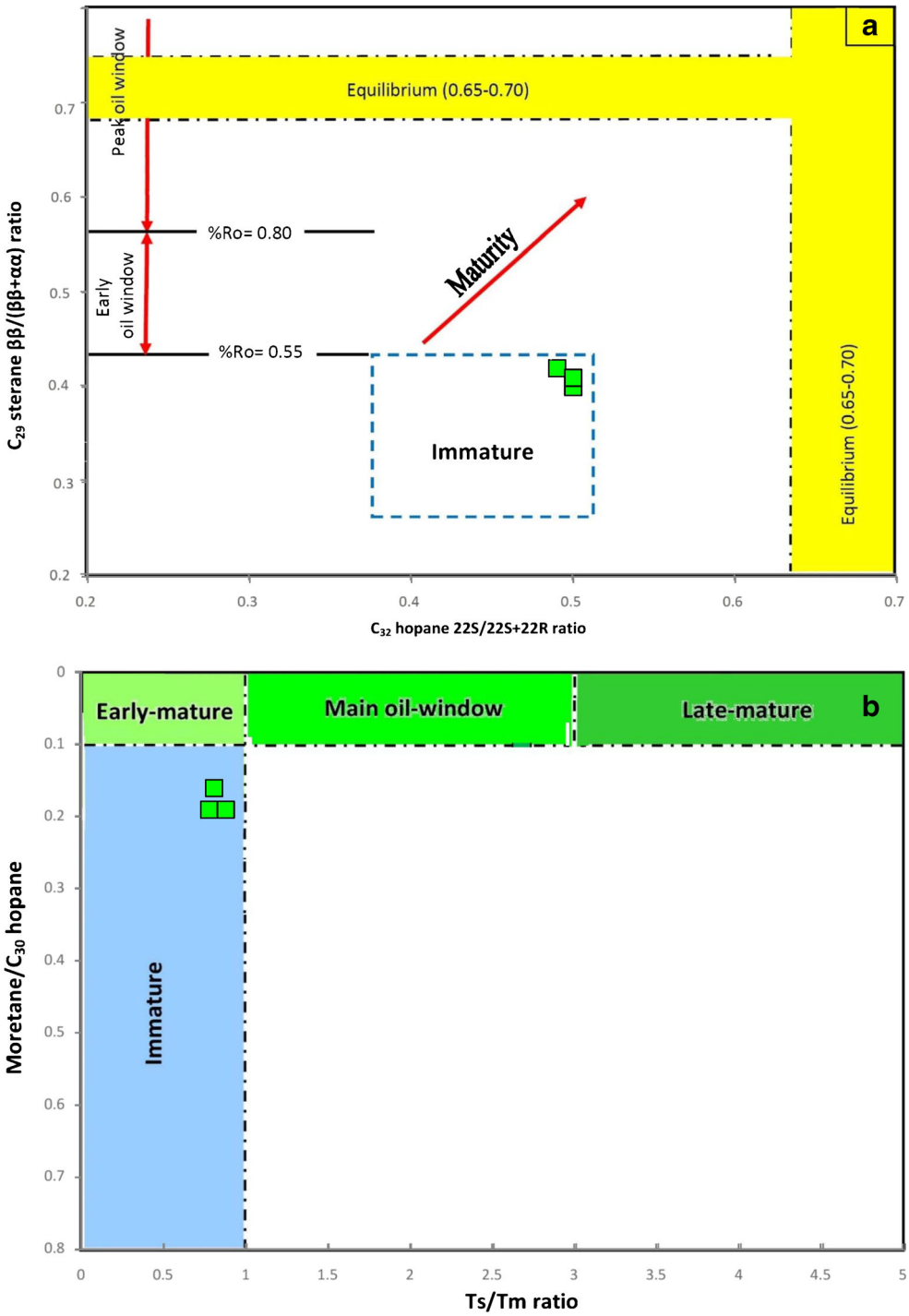

Fig. 13 Immature source rock range of the analyzed shale samples, determined from various biomarker maturity parameters: (**A**) the ββ/(αα+ββ) ratio of C_{29} sterane and the 22S/(22S+22R) ratio of C_{32} hopane, and (**B**) the Ts/Tm and moretane/hopane ratios. This interpretation is based on Mackenzie et al. (1980) and Seifert and Moldowan (1986)

The C_{32} 20S/(20S+20R) ratio of more than 0.50 suggests material reaching oil window maturity (Seifert and Moldowan 1986). The C_{32} hopane ratio in the analyzed shale samples ranged from 0.49 to 0.50, indicating that the organic matter in these sediments is approaching the oil window maturity.

Some aliphatic parameters, namely, the ββ/(ββ + αα) and 20S/(20S + 20R) ratios of C_{29} sterane were also used as maturity indicators (Seifert and Moldowan 1978, 1981, 1986). The C_{29} 20S/(20S+20R) and ββ/(ββ+αα) sterane ratios for three extracted rock samples were calculated have the low values in the ranges of 0.30–0.40 and 0.40–0.42, respectively (Table 2). Together with the C_{29} sterane ββ/(ββ +αα)) ratio, the C_{32} hopane ratio suggests immature organic matter in the analyzed shales (Fig. 13A). This immature stage is consistent with the values of Ts/Tm and CM_{30}/C_{30} ratios (Fig. 13B). Consequently, immature stage implied by the biomarker ratios

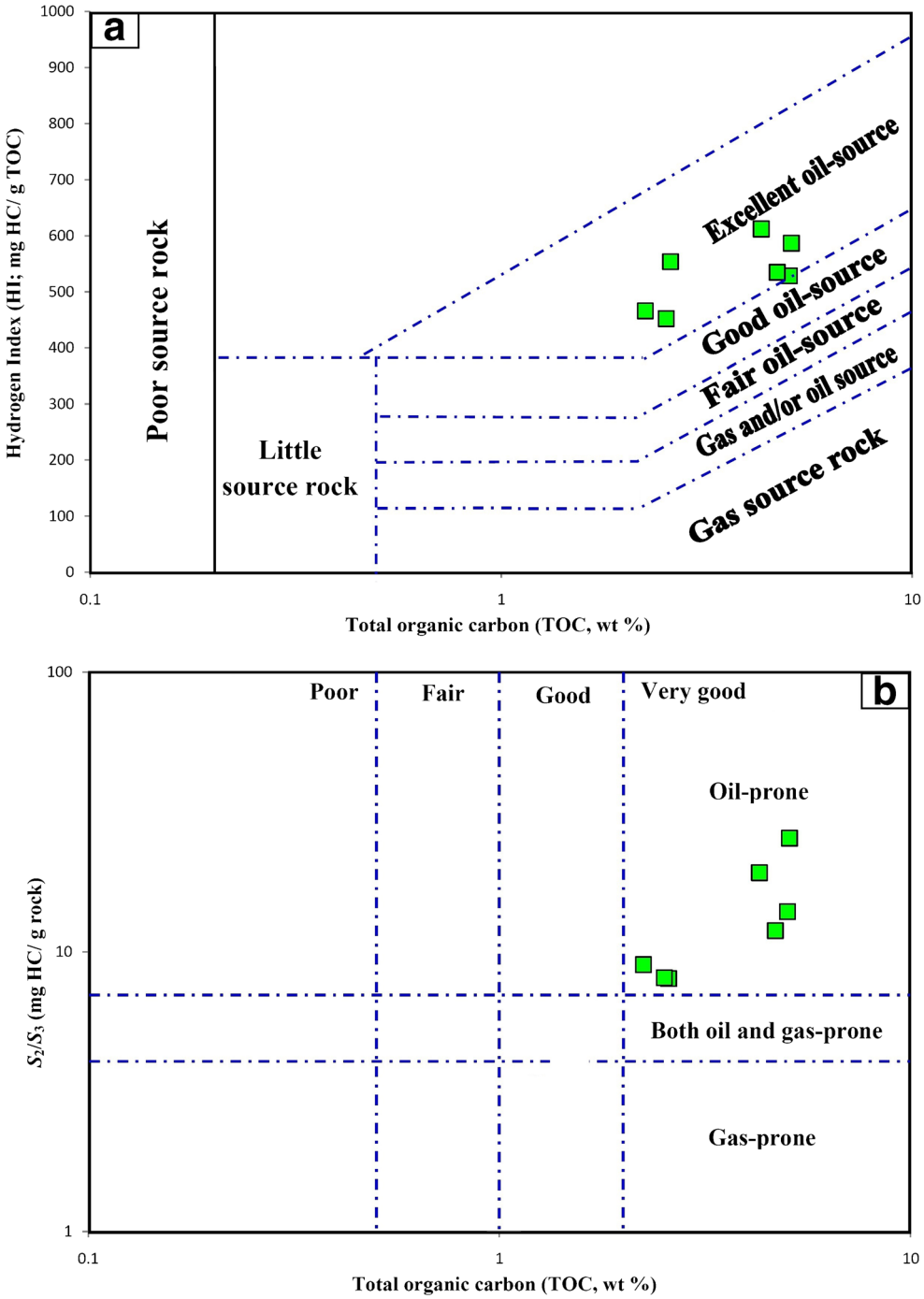

Fig. 14 Geochemical correlations between TOC content and Rock-Eval data (the HI and S2/S3 parameters), implying that the Galhak shales are very good source rocks for oil generation in the northern Melut Basin, Sudan

and low VRs (<0.50%) is incompatible with relatively high T_{max} values (Table 1). The high T_{max} values of the analyzed samples could be attributed to the interference in the muddy–silty rich mineral matrix (Espitalié et al. 1980; Peters 1986). This suggestion is supported by the significantly reduced amounts of pyrolytic effluents (S_2) adsorbed by clay minerals in the analyzed shale samples (Espitalié et al. 1980; Peters 1986). Therefore, the T_{max} data are probably inaccurate for assessing the thermal maturation of the analyzed samples.

Petroleum generation potential

The potential of petroleum generation is generally evaluated based on the organic facies of the kerogen dispersed in the source rock and their maturation level (e.g., Dow 1977; Peters and Cassa 1994; Abdullah et al. 2017). In the current study, geochemical results were integrated with the visual kerogen microscopy and used to discuss the characteristics of the kerogen of the analyzed Galhak shale samples and predict their potential as a petroleum resource in the northern Melut Basin,

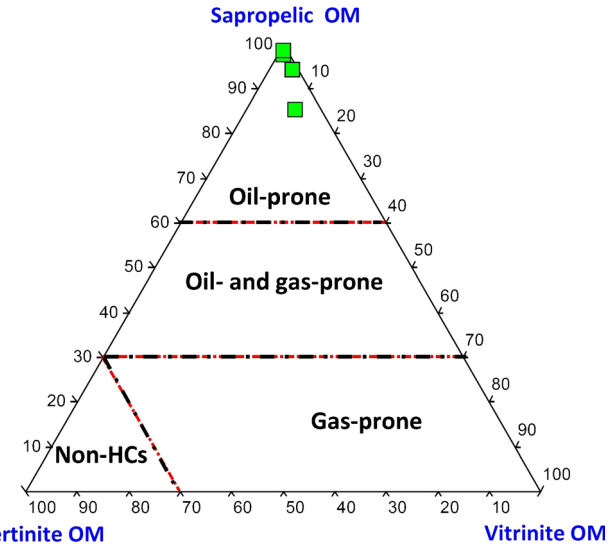

Fig. 15 Ternary plot of the dominant kerogen assemblages recognized in the samples from the well in Galhak shale, showing oil that will likely be generated in the mature shales

Sudan. The geochemical results of Rock-Eval pyrolysis, with HI values more than 400-mg HC/g TOC predict that the organic matter type of the Galhak shale samples under study is mainly types I and III kerogen (Fig. 5). The organic facies of high proportions of type I and II kerogens suggest primarily sapropel derived from algal organic matter as demonstrated by the organic biomarkers and kerogen microscopy results. These shale sediments of the Galhak Formation under study contain high proportions of type I and II kerogens that can generate notable amounts of oil. This conclusion can also be deduced from the chemical correlations between the TOC content and the S_2/S_3 and HI Rock-Eval parameters (Fig. 14). The potential for hydrocarbon generation of mainly oil from the Galhak shale also conforms from the microscopic kerogen assemblages plotted on a Tissot and Welte (1978) ternary diagram (Fig. 15).

Beside the organic facies of the kerogen, the petroleum generation potential was further assessed from the thermal alteration of organic matter in the analyzed Galhak shale samples. In agreement with previously obtained maturity data, these shale sediments from the studied well in the northern Melut Basin generally represent immature source rocks and have not yet reached oil-window maturity level. Accordingly, the Galhak source-rock containing types I and II kerogen in the deeper well locations in the Melut Basin may be sufficiently mature of peak oil-window and could lead to lucrative oil generation.

Conclusions

Organic geochemical and microscopic investigations were performed on organic-rich shales of the Late Cretaceous Galhak Formation. Samples were collected from one well in the northern Melut Basin, Sudan. The main conclusions are outlined below.

1- The TOC contents of the Galhak shales all exceeded 2%, indicating that the shales are favorable source rocks for prospecting.
2- The Galhak organic-rich shales contain high levels of aquatic-derived sapropel or sapropelite and were classified as hydrogen-rich types I and II kerogen, with HI values between 452 and 612 mg HC/g TOC. Thus, they can potentially generate commercial amounts of oil.
3- The biomarker distributions revealed that the Galhak oil-prone shales were deposited in a relatively fresh lacustrine environment under suboxic to relatively oxic conditions. High contributions of algal organic matter with few plant inputs were accumulated during the deposition.
4- The biomarkers and the optical and chemical maturity data further confirm immature organic matter in the Galhak shales. Oil has not yet been generated at the current shallow burial depth.
5- These conclusions enhance the prospects and exploration strategies for commercial oil generation and production along deep parts of the Melut Basin, where these organic-rich shales could reach a good maturity level.

Appendix

Table 3 Peak assignments for hydrocarbons in the gas chromatograms of saturated fractions in the m/z 191 (I) and 217 (II) mass fragmentograms (use for reference to explain Fig. 9).

(I) Peak *no.*	Compound abbreviation	
Ts	18α(H),22,29,30-trisnorneohopane	Ts
Tm	17α(H),22,29,30-trisnorhopane	Tm
29	17α,21β(H)-nor-hopane	C_{29} hop
30	17α,21β(H)-hopane	Hopane
30M	17 β,21α (H)-Moretane	C_{30}Mor
31S	17α,21β(H)-homohopane (22S)	C_{31}(22S)
31R	17α,21β(H)-homohopane (22R)	C_{31}(22R)
32S	17α,21β(H)-homohopane (22S)	C_{32}(22S)
32R	17α,21β(H)-homohopane (22R)	C_{32}(22R)
33S	17α,21β(H)-homohopane (22S)	C_{33}(22S)
33R	17α,21β(H)-homohopane (22R)	C_{33}(22R)
34S	17α,21β(H)-homohopane (22S)	C_{34}(22S)
34R	17α,21β(H)-homohopane (22R)	C_{34}(22R)
35S	17α,21β(H)-homohopane (22S)	C_{35}(22S)
35R	17α,21β(H)-homohopane (22R)	C_{35}(22R)
(II) Peak *no.*		
a	13β,17α(H)-diasteranes 20S	Diasteranes
b	13β,17α(H)-diasteranes 20R	Diasteranes
c	13α,17β(H)-diasteranes 20S	Diasteranes
d	13α,17β(H)-diasteranes 20R	Diasteranes
e	5α,14α(H), 17α(H)-steranes 20S	ααα20S
f	5α,14β(H), 17β(H)-steranes 20R	αββ20R
g	5α,14β(H), 17β(H)-steranes 20S	αββ20S
h	5α,14α(H), 17α(H)-steranes 20R	ααα20R

Acknowledgements The authors would like to thank and appreciate the Ministry of Energy and Mining of Sudan for their helping and giving the data for this research. The authors also extend their sincere appreciation to the Deanship of Scientific Research at King Saud University for funding the work. The constructive comments by an Associate Editor Dr. Barry Katz and an anonymous reviewer that improved the original manuscript are gratefully acknowledged.

Declarations

Conflict of interest The authors declare that they have no competing interests.

References

Abdullah WH, Togunwa QS, Makeen YM, Hakimi MH, Mustapha KA, Baharuddin MH, Sia SG, Tongkul F (2017) Hydrocarbon source potential of Eocene-Miocene sequence of western Sabah, Malaysia. Mar Petrol Geol 83:345–361

Binks RM, Fairhead JD (1992) A plate tectonic setting for the Mesozoic rifts of Western and Central Africa. In: Ziegler PA (ed) Geodynamics of rifting, volume II. Case History Studies on Rifts North and South America, Tectonophysics, vol 213, pp 141–151

Bissada KK (1982) Geochemical constraints on petroleum generation and migration—a review. Proc ASCOPE Conf 81:69–87

Bordenave ML, Espitalie J, Leplat P, Oudin JL, Vendenbroucke M (1993) Screening techniques for source rock evaluation. In: Bordenave ML (ed) Applied Petroleum Geochemistry Editions Technip, Paris, pp 237–255

Browne S, Fairhead J, Mohamed I (1985) Gravity study of the White Nile Rift, Sudan, and its regional tectonic setting. Tectonophysics 113: 123–137

Burwood R, Leplat P, Mycke B, Paulet J (1992) Rifted margin source rock deposition: a carbon isotope and biomarker study of a West African lower cretaceous "Lacustrine" section. Org Geochem 19(1-3):41–52

Chandra K, Mishra CS, Samanta U, Gupta A, Mehrotra KL (1994) Correlation of different maturity parameters in the Ahmedabad–Mehsana Block of the Cambay Basin. Org Geochem 21:313–321

Cornford C (1979) Organic deposition at a continental rise; organic geochemical interpretations and synthesis at DSDP Site 397, eastern North Atlantic. Init. Repts. Deep Sea Drilling Projects 47:503–510

Dembicki HJ (2009) Three common source rock evaluation errors made by geologists during prospect or play appraisals. Am Assoc Pet Geol Bull 93(3):341–356

Didyk BM, Simoneit BRT, Brassell SC, Eglinton G (1978) Organic geochemical indicators of palaeoenvironmental conditions of sedimentation. Nature 272:216–222

Dou L, Xiao K, Cheng D, Shi B, Li Z (2007) Petroleum geology of the Melut Basin and the Great Palogue Field, Sudan. Mar Pet Geol 24: 129–144

Dou C, Dingsheng L, Zhiwei Z, Jingchun W (2013) Petroleum geology of the Fula-sub Basin, Muglad Basin, Sudan. J Pet Geol 36:43–60

Dow WG (1977) Kerogen studies and geological interpretations. J Geochem Explor 7:79–99

El Nady MM, Harb FM, Mohamed NS (2014) Biomarker characteristics of crude oils from Ashrafi and GH oilfields in the Gulf of Suez, Egypt: an implication to source input and paleoenvironmental assessments. Egypt J Pet 23:455–459

Espitalie J, Laporte L, Madec M, Marquis F, Leplate P, Pault J, Boutefeu A (1977) Methode rapid de caracterisation des rocks meres, deleur potential petrolier et leurdegre devolution. Rev Inst Fr Petrol 32:23–42

Espitalié J, Madec M, Tissot B (1980) Role of mineral matrix in kerogen pyrolysis: influence on petroleum generation and migration. Am Assoc Pet Geol Bull 64:59–66

Espitalie J, Deroo G, Marquis F (1985) La pyrolyse rock-eval et ses applications. Partie 1. Revue de 1'lnstitut Francois du Petrole 40(5):563–579

Fatma H, Sadettin K (2013) Organic geochemistry and depositional environments of Eocene coals in northern Anatolia Turkey. Fuel 113: 481–496

Genik GJ (1993) Petroleum geology of Cretaceous-Tertiary rift basins in Niger, Chad and Central African Republic. AAPG Bull 77, 1405–1434

Guiraud R, Maurin JC (1992) Early Cretaceous rift of Western and Central Africa: an overview. Tectonophysics 213:153–168

Gürgey K (1999) Geochemical characteristics and thermal maturity of oils from the Thrace Basin (western Turkey) and western Turkmenistan. J Pet Geol 22:167–189

Hakimi MH, Abdullah WH, Shalaby MR (2012) Molecular composition and organic petrographic characterization of Madbi source rocks from the Kharir Oilfield of the Masila Basin (Yemen): palaeoenvironmental and maturity interpretation. Arab J Geosci 5(4):817–831

Hakimi MH, Ahmed AF, Abdullah WH (2016) Organic geochemical and petrographic characteristics of the Miocene Salif organic-rich shales in the Tihama Basin, Red Sea of Yemen: implications for paleoenvironmental conditions and oil-generation potential. Int J Coal Geol 154-155:193–204

Hakimi MH, Al-Matary AM, El-Mahdy O, Hatem BA, Kahal AY, Lashin A (2020) Organic geochemistry characterization of Late Jurassic bituminous shales and their organofacies and oil generation potential in the Shabwah depression, southeast Sabatayn, Yemen. J Pet Sci Eng 188:106951

Hanson AD, Zhang SC, Moldowan JM, Liang DG, Zhang BM (2000) Molecular organic geochemistry of the Tarim basin, NW China. Am Assoc Petrol Geol Bull 84:1109–1128

Huang WY, Meinschein WG (1979) Sterols as ecological indicators. Geochim Cosmochim Acta 43:739–745

Katz B, Lin F (2014) Lacustrine basin unconventional resource plays: key differences. Mar Pet Geol 56:255–265

Mackenzie AS, Patience RL, Maxwell JR, Vandenbroucke M, Durand B (1980) Molecular parameters of maturation in the Toarcian shales, Paris Basin, France—I. Changes in the configurations of acyclic isoprenoid alkanes, steranes and triterpanes. Geochim Cosmochim Acta 44:1709–1721

Makeen YM, Abdullah WH, Hakimi MH (2015a) Biological markers and organic petrology study of organic matter in the Lower Cretaceous Abu Gabra sediments (Muglad Basin, Sudan): origin, type and palaeoenvironmental conditions. Arab J Geosci 8:489–506

Makeen YM, Abdullah WH, Hakimi MH, Mustapha KA (2015b) Source rock characteristics of the lower cretaceous Abu Gabra Formation in the Muglad Basin, Sudan, and its relevance to oil generation studies. Mar Pet Geol 59:505–516

Makeen YM, Abdullah WH, Pearson MJ, Hakimi MH, Elhassan OMA, Yousif TAH (2016a) Thermal maturity history and petroleum generation modelling for the lower cretaceous Abu Gabra Formation in the Fula sub-basin, Muglad Basin, Sudan. Mar Pet Geol 75:310–324

Makeen YM, Abdullah WH, Pearson MJ, Hakimi MH, Ayinla HA, Elhassan OMA, Abas AM (2016b) History of hydrocarbon generation, migration and accumulation in the Fula sub-basin, Muglad Basin, Sudan: implications of a 2D basin modeling study. Mar Pet Geol 77:931–941

Marynowski L, Narkiewicz M, Grelowski C (2000) Biomarkers as environmental indicators in a carbonate complex, example from the Middle to Upper Devonian, Holy Cross Mountains, Poland. Sediment Geol 137(3-4):187–212

McHargue TR, Heidrick JL, Livingstone JE (1992) Tectono-stratigraphic development of the interior Sudan rifts, Central Africa. Tectonophysics 213:187–202

Mohamed AY, Pearson MJ, Ashcroft WA, Iliffe WA, Whiteman AJ (1999) Modelling petroleum generation in the southern Muglad Rift Basin Sudan. AAPG Bull 83:1943–1964

Mohamed AY, Iliffe JE, Ashcroft WA, Whiteman AJ (2000) Burial and maturation history of the Heglig field area, Muglad Basin, Sudan. J Pet Geol 23(1):107–128

Mohamed AY, Pearson MJ, Ashcroft WA, Whiteman AJ (2002) Petroleum maturation modelling, Abu Gabra–Sharaf area, Muglad Basin Sudan. J Afr Earth Sci 35:331–344

Moldowan JM, Sundararaman P, Schoell M (1985) Sensitivity of biomarker properties to depositional environment and/or source input in the Lower Toarcian of S.W. Germany. Org Geochem 10:915–926

Mukhopadhyay PK, Wade JA, Kruge MA (1995) Organic facies and maturation of Jurassic/Cretaceous rocks, and possible oil-source rock correlation based on pyrolysis of asphaltenes, Scotion Basin, Canada. Org Geochem 22:85–104

Peters KE (1986) Guidelines for evaluating petroleum source rock using programmed pyrolysis. Am Assoc Pet Geol Bull 70:318–329

Peters K, Cassa M (1994) Applied Source Rock Geochemistry. In Magoon, L.B. and Dow, W. G. eds., 1994, The petroleum system from source to trap. AAPG Mem 60:93–117

Philp RP (1985) Biological markers in fossil fuel production. Mass Spectrom Rev 4:1–54

Roushdy MI, El Nady MM, Mostafa YM, El Gendy NS, Ali HR (2010) Biomarkers characteristics of crude oils from some oilfields in the Gulf of Suez, Egypt. J Am Sci 6:911–925

Schull TJ (1988) Rift basins of interior Sudan: petroleum exploration and discovery. Am Assoc Pet Geol Bull 72:1128–1142

Seifert WK, Moldowan JM (1978) Application of steranes, terpanes and monoaromatic to the maturation, migration and source of crude oils. Geochim Cosmochim Acta 42:77–95

Seifert WK, Moldowan JM (1981) Palaeoreconstruction by biological markers. Geochim Cosmochim Acta 45:783–794

Seifert WK, Moldowan JM (1986) Use of biological markers in petroleum exploration. In: Johns RB. editor. vol. 24. Amsterdam: Methods in Geochemistry and Geophysics Book Series, pp. 261–90

Sinninghe Damsté JS, Kenig F, Koopmans MP, Koster J, Schouten S, Hayes JM, de Leeuw JW (1995) Evidence for gammacerane as an indicator of water column stratification. Geochim Cosmochim Acta 59:1895–1900

Sweeney JJ, Burnham AK (1990) Evaluation of a simple model of vitrinite reflectance based on chemical kinetics. AAPG Bull 74: 1559–1570

Taylor GH, Teichmüller M, Davis A, Diessel CFK, Littke R, Robert P (1998) Organic petrology. Gebrüder Borntraeger, Stuttgart

Teichmüller M, Littke R, Robert P (1998) Coalification and maturation. In: Taylor GH, Teichmüller M, Davis A, Diessel CF, Littke R, Robert P (eds) Organic petrology. Gebrüder Borntraeger, Berlin, pp 86–174

ten Haven HL, Rohmer M, Rullkotter J, Bisseret P (1989) Tetrahymanol, the most likely precursor of gammacerane, occurs ubiquitously in marine sediments. Geochim Cosmochim Acta 53:3073–3079

Tissot BP, Welte DH (1978) Petroleum formation and occurrence. Springer, New York

Tissot BP, Pelet R, Ungerer PH (1987) Thermal history of sedimentary basins, maturation indices, and kinetics of oil and gas generation. AAPG Bull 71:1445–1466

Tong X, Dou L, Tian Z, Pan X, Zhu X (2004) Geological mode and hydrocarbon accumulating mode in Muglad passive Rift Basin, Sudan. Acta Pet Sin 25(1):19–24

Volkman JK (1986) A review of sterol biomarkers for marine and terrigenous organic matter. Org Geochem 9:83–89

Waples DW (1994) Modeling of sedimentary basins and petroleum systems. In: Magoon LB, Dow WG (eds) The petroleum system from source to trap: AAPG Mem, vol 60, pp 307–322

Waples DW, Machihara T (1991) Biomarkers for geologists–a practical guide to the application of steranes and triterpanes in petroleum geology: Association of Petroleum Geologists, Methods in Exploration No. 9, 91 p